Unleashing the Power of Coherent Optical Technology

Revolutionizing Next-Generation PONs with Flexible Rates, Upstream Burst Detection, and Network Protection

A Technical Paper prepared for presentation at SCTE TechExpo24

Haipeng Zhang, Ph.D.
Principal Architect
CableLabs
858 Coal Creek Circle, Louisville CO, 80027
303.661.3796
h.zhang@cablelabs.com

Zhensheng (Steve) Jia, Ph.D.
Fellow and Director of Advanced Optical Technologies
CableLabs
858 Coal Creek Circle, Louisville CO, 80027
303.661.3364
s.jia@cablelabs.com

L. Alberto Campos, Ph.D.
Fellow
CableLabs
858 Coal Creek Circle, Louisville CO, 80027
303.661.3377
a.campos@cablelabs.com

Table of Contents

List of Figures

List of Tables

Title **Page Number**

1. Introduction and Motivation

The demands for increased capacity, speed, reliability, and coverage in access networks are ever-growing, driven by the proliferation of high-bandwidth applications and services. Passive optical networks (PON) play a crucial role in meeting these demands due to their efficiency and cost-effectiveness [1-3]. A PON is a point-to-multipoint optical network architecture that utilizes passive components in the field, forming an optical distribution network that supports multiple end-users effectively. This architecture is instrumental in delivering high-speed internet and other communication services, making it a backbone for modern optical access networks. Several generations of PON systems have been standardized through the efforts of the International Telecommunication Union Telecommunication Standardization Sector (ITU-T) and the IEEE 802.3 Ethernet Working Group [4-6]. These advancements highlight the continuous evolution and adaptation of PON technology to meet the growing demands of modern optical access networks.

As the industry progresses toward 100G capacity and beyond in PON, intensity-modulation direct-detection (IM-DD) technology faces significant challenges due to its limited power budget, capacity, and susceptibility to fiber impairments. In contrast, coherent technology offers higher receiver sensitivity, supports advanced modulation formats, and provides a larger link budget, making it more suitable for future PON applications. Coherent optics, once limited to long-haul networks, are now expanding into short-haul and access networks, paving the way for future generation optical access networks.

In this work, we showcase the great potential of CPON technology in terms of cost reduction, flexibility, and survivability. By demonstrating key innovations such as low-cost ONU designs, efficient upstream burst processing, adaptive modulation, flexible data rates, and innovative protection schemes, we want to show how CPON can provide a robust and scalable solution for the next generation of optical access networks.

1.1. Passive Optical Network Overview

Traditional PON systems, based on intensity modulation-direct detection (IM-DD) technology which modulates the intensity of the optical signal for data transmission, are widely deployed in today's access networks due to their cost-effectiveness and simplicity. Utilizing a point-to-multipoint architecture, a single optical line terminal (OLT) at the central office (or remote locations for remote OLT use cases) connects to multiple optical network units (ONUs) or optical network terminals (ONTs), which are typically located at the end user's premises, through a passive optical link. In this work, the term 'ONU' will be employed henceforth to refer to customer premise devices.

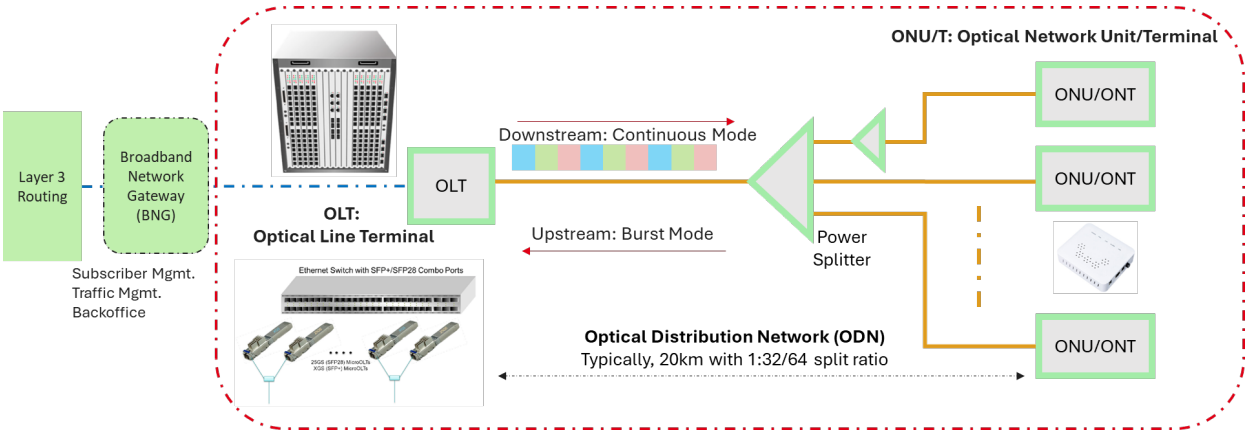

Figure 1 – Passive optical network architecture

Figure 1 illustrates a typical architecture of a PON system, detailing the flow of data between various network components. The OLT, positioned at the central office, sends Ethernet data to ONUs in broadcast mode, initiates and controls the ranging process, and allocates bandwidth by controlling ONU transmission window. The optical distribution network (ODN) is composed of an optical fiber link and passive optical splitters that distribute the optical signals from the OLT to multiple ONUs . In the downstream (DS) direction, data is broadcast continuously from the OLT to the ONUs. For the upstream (US) direction, data is transmitted from ONUs to the OLT in bursts, allowing efficient sharing of bandwidth in the time domain.

1.2. Coherent Optical Technology for Next-Generation PON

As the industry progresses towards next-generation PON requiring 100G or higher bandwidth, IM-DD technology encounters significant challenges due to its inherent limitations. These include a restricted power budget, limited capacity, and vulnerability to fiber impairments such as chromatic dispersion (CD). To address these issues, IM-DD would require the integration of additional components like analog-digital convertor (ADC)/ digital-analog convertor (DAC), high-speed and high-sensitivity photodiodes, CD mitigation technologies, and extremely high transmitter output power in the range of 8 dBm to 11 dBm to achieve anticipated link budget requirements for next-generation PON. Such enhancements would inevitably increase the cost and complexity of existing IM-DD PON systems.

In contrast, coherent technology offers several advantages for 100G PON and beyond. It provides high receiver sensitivity, supports advanced modulation formats for higher capacity, and boasts a large link budget that allows for extended reach and higher splitting ratios. Moreover, coherent technology possesses powerful digital signal processing (DSP) capabilities that effectively counteract fiber impairments [7, 8]. Although the cost of coherent optics is higher today compared with IM-DD technology, its benefits make it a more optimized and extensible solution for future PON applications. The evolution of coherent optics, traditionally used in long-haul and metro applications, has now expanded to new market segments, including short-haul applications in edge and access networks. Future trends in coherent optical networking encompass intra-data center communication and point-to-multipoint PONs. Figure 1 illustrates the technological paths of IM-DD and coherent technology towards next-generation 100G PON applications.

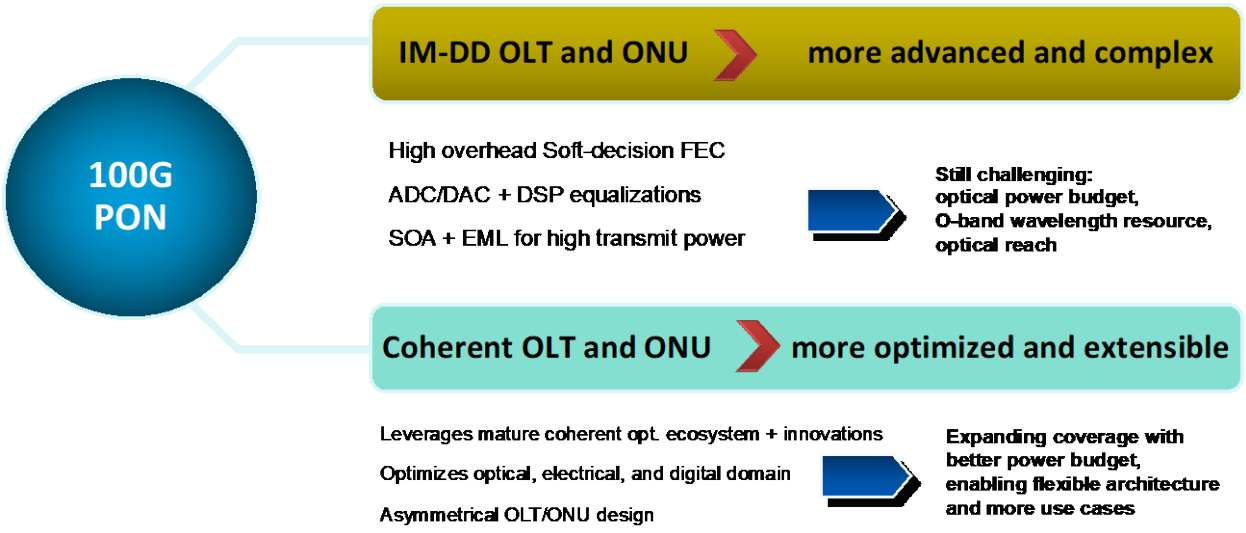

Figure 2 – Next generation 100G PON technology paths

In response to these advancements, CableLabs launched the 100G Coherent PON (CPON) initiative in 2021, aiming to support future capacity and service requirements, and ensuring that CableLabs members are equipped with the bandwidth and tools needed to lead the broadband industry. In 2023, ITU-T also initiated the development of the [118-WP1] G.Sup.VHSP Draft, focusing on passive optical access system requirements and transmission technologies exceeding 50 Gbit/s per wavelength, with coherent technology as one of the options under consideration. This ongoing work signifies the importance and potential of coherent technology in shaping the future of high-capacity optical access networks.

1.3. Coherent PON Architectures

As noted above, Coherent PON is being developed to address demand for higher capacity, longer reach, and better spectral efficiency in optical access networks. Various coherent PON architectures have been explored and demonstrated, including wavelength division multiplexing (WDM) PON, time division multiplexing (TDM) PON, and time-and frequency- division multiplexing (TFDM) PON [9-14]. In this article, we will focus on the latter two architectures, TDM and TFDM coherent PON, which are depicted in Figure 3.

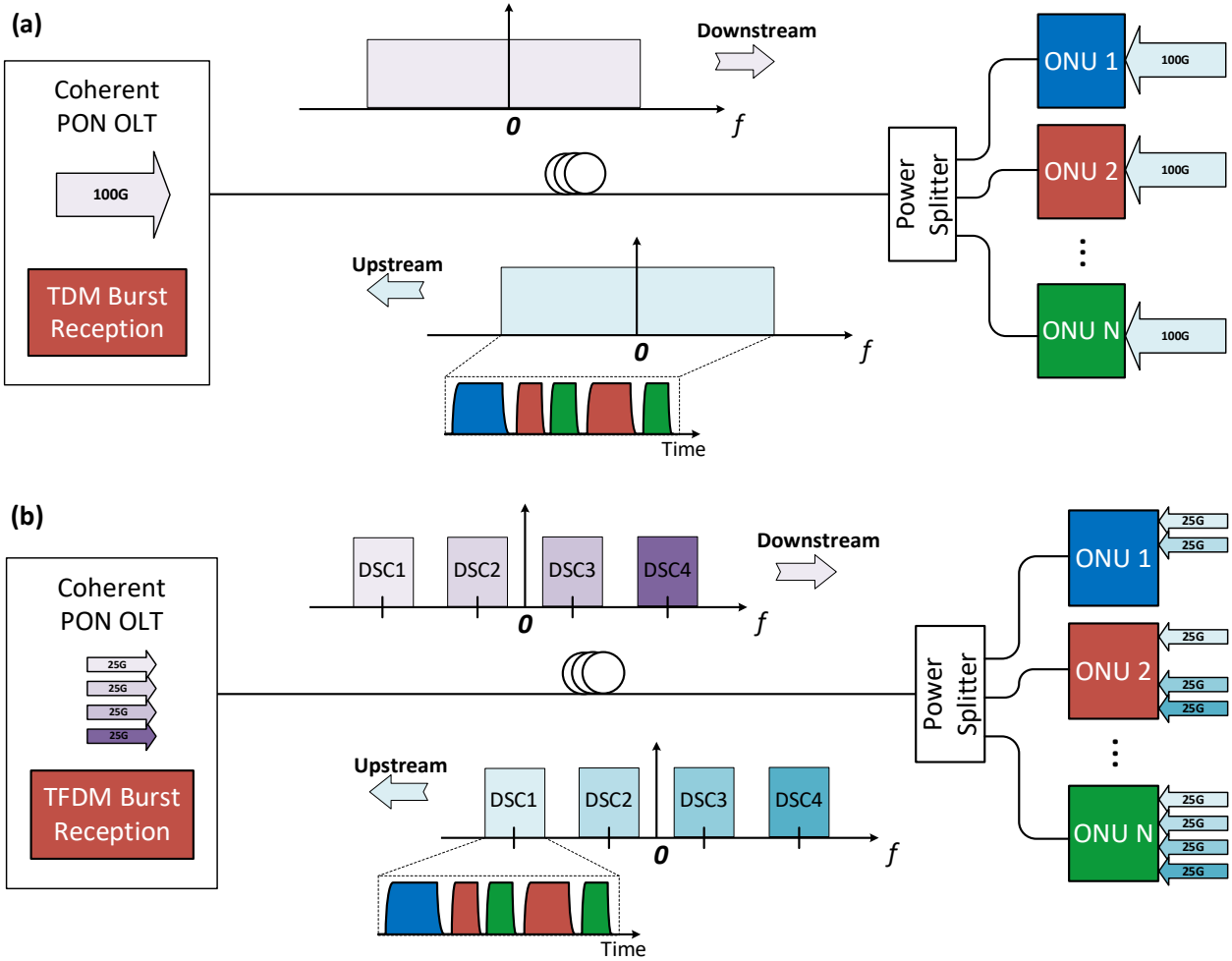

Figure 3 – CPON technology options: (a) TDM CPON; (b) TFDM CPON

In the TDM Coherent PON architecture, as shown in Figure 3(a), a single optical carrier is used for DS transmissions, while a distinct optical carrier operating at a different wavelength is employed for US

transmission. The OLT operates with a TDM burst receiver. DS data is transmitted continuously from the OLT to multiple ONUs through an ODN that consists of a fiber link and passive optical splitters, with each ONU receiving the same DS signal. For US transmission, ONUs send data in distinct time slots to avoid collision, effectively sharing the same wavelength in a time-multiplexed manner.

In contrast, the TFDM Coherent PON architecture illustrated in Figure 3(b) combines both time and frequency division multiplexing. The OLT employs a TFDM burst receiver, and data is carried by multiple digital subcarriers (DSCs), which are transmitted DS simultaneously in different frequency bands in continuous mode. For US transmission, ONUs similarly send data over designated DSCs, and within each DSC different ONUs can send data in distinct time slots. In addition to the inherent advantages of coherent technology, TFDM technology also utilizes the frequency domain to further enhance network flexibility and can offer dedicated DSC for certain applications.

Both TDM and TFDM Coherent PONs provide scalable and flexible solutions for future optical access networks. The TDM approach offers a simpler solution as it does not require frequency division processing and channel-bonding capability in the management layer. In contrast, TFDM Coherent PON offers a higher degree of flexibility but comes at the cost of additional complexity and higher costs due to the need for advanced frequency division processing and channel management capabilities. In this article, we will showcase the latest developments in both TDM and TFDM Coherent PONs and discuss several enabling technologies such as cost reduction leveraging optical injection locking, upstream burst transmission, flexible data rate, and coherent PON protection.

2. Cost Reduction in Coherent PON

Coherent solutions are expanding from long-haul and metro networks to data center interconnect (DCI) and access networks, driven by the increasing needs in bandwidth. However, the high cost of coherent optics, mainly due to complex components like tunable lasers, local oscillators, and DSP chips, remains a challenge for large-scale deployments in short-haul networks. In the access environments, cost-effective lasers with acceptable performance degradation are preferred over the high-cost external cavity lasers (ECLs) used in long-haul systems. This section will explore an approach for utilizing lower cost lasers in a Coherent PON system.

2.1. Optical Injection Locking

Optical injection locking (OIL) is a well-known phenomenon where a laser diode (referred to as the child laser) becomes phase and frequency locked to an external signal originating from a free-running laser (known as the parent laser) [15-17]. By applying frequency and phase locking, a simple and cost-effective multi-mode Fabry-Perot laser diode (FP-LD) can be transformed into single-mode operation through injection of a high-quality single-mode signal into its cavity. Leveraging OIL, several fundamental limitations of basic FP lasers can be addressed, including achieving single-mode operation, side-mode suppression, enhanced modulation bandwidth, reduced nonlinear distortion, and minimized intensity noise and chirp. Figure 4(a) illustrates the schematic setup of an OIL system, where the parent laser (typically an external cavity laser) injects light into the FP-LD via a three-port optical circulator, and the FP-LD output exits through the same optical circulator. This laser design feature is commonly found in commercial products.

In our experimental setup, a C-band ECL serves as the master source, with adjustable output power ranging from 6 dBm to 15 dBm. The child lasers are FP-LDs housed in 7-pin butterfly packages, featuring a cavity length of approximately 350 μm and a maximum output power of up to +14 dBm. When the wavelength of the parent laser falls within a specific frequency detuning range relative to the child laser, the child laser's wavelength is pulled toward the master's wavelength. Eventually, the laser

dynamics settle, achieving both frequency and phase locking to the parent laser. Figures 4(b) and 4(c) depict the optical spectrum of the FP-LD before and after injection locking, respectively. With a spectral linewidth matching that of the seed ECL light, the injection-locked FP-LD can serve as a coherent light source for signal generation and detection.

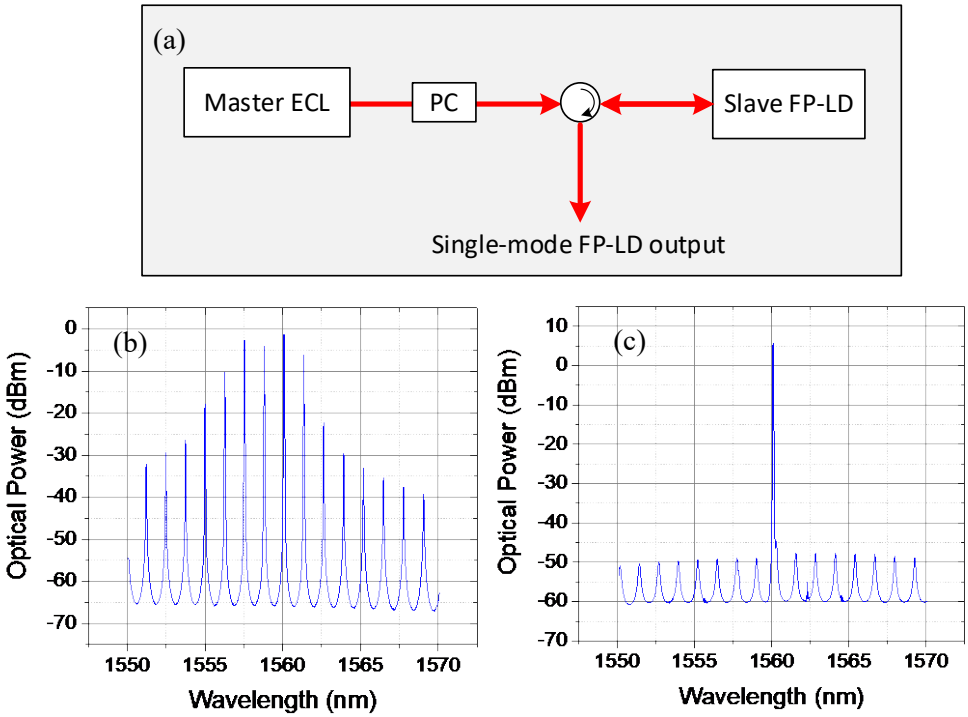

Figure 4 – Optical injection locking setup (a), and slave FP laser spectrum before injection locking (b), after injection locking (c)

Frequency detuning, a critical factor influencing the stability and reliability of OIL, pertains to the frequency difference between the ECL and the FP-LD modes. Remarkably, OIL does not necessitate perfect mode overlap between the ECL and any specific FP-LD mode. Even under diverse injection conditions, successful injection locking can be achieved despite frequency detuning. Our experimental investigation involved varying injection ratios and detuning frequencies. Figure 5(a) illustrates the injection locking map, where the ECL frequency is adjusted to introduce detuning from an FP-LD cavity mode. The injection ratio, defined as the master ECL output power relative to the unchanged +5 dBm slave FP-LD power, was varied using a variable optical attenuator. The blue dots in Figure 5(a) correspond to successful injection locking instances at specific injection ratios and detuning frequencies. At high injection ratios, OIL is more forgiving of frequency detuning, while at low ratios, precise alignment of the ECL frequency with the FP-LD mode is necessary. Our experimental findings align well with theoretical calculations and previous reports [15, 16]. Notably, the detuning frequency range exhibits asymmetry relative to the FP-LD side mode center frequency, with greater tolerance for detuning on the longer-wavelength (lower-frequency) side.

The side mode suppression ratio (SMSR) of the injection-locked FP-LD is investigated under various frequency detuning conditions at an injection ratio of 10 dB, as depicted in Figure 5(b). When experiencing positive frequency detuning, the SMSR tends to decrease with increasing detuning. Conversely, under negative frequency detuning, the SMSR initially improves with increasing detuning but eventually decreases after reaching a certain level. This asymmetry in SMSR, together with the asymmetry in the frequency detuning range, can be attributed to the linewidth enhancement factor of the

parent laser, which introduces carrier variation and causes a shift in the child FP-LD laser gain towards longer wavelengths [15, 16].

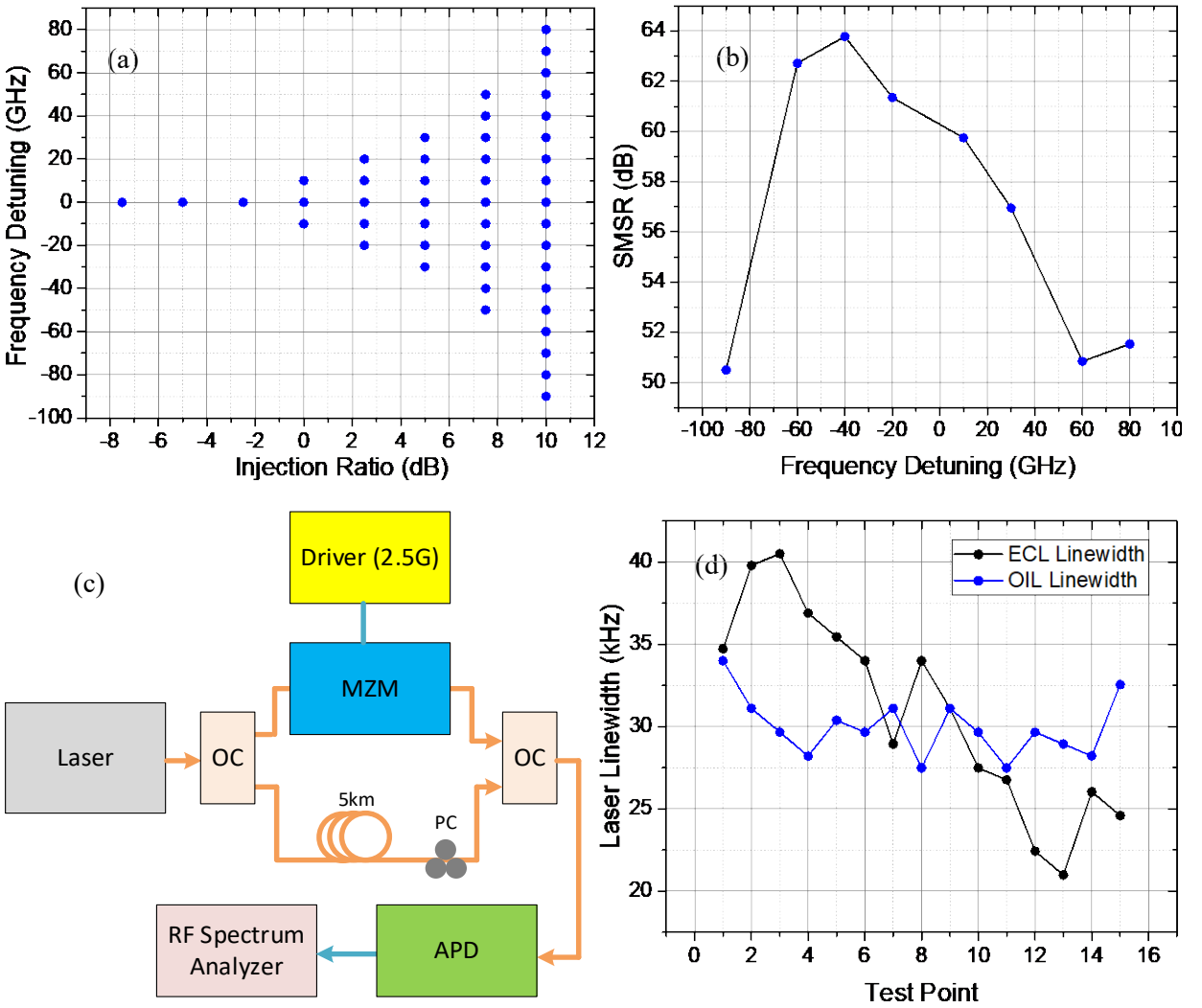

Figure 5 – Optical injection locking: (a) injection locking map under various injection ratio and frequency detuning; (b) SMSR of the FP-LD under various frequency detuning; (c) delayed self heterodyne laser linewidth measurement setup; (d) measured linewidth of ECL and injection locked FP-LD

The laser linewidth significantly impacts coherent optical communication systems. To measure the laser linewidth, we employed a delayed self-heterodyne measurement setup, as shown in Figure 5(c). Both the injection-locked FP-LD and a high-quality ECL were evaluated. The light from the source under test (either the OIL FP-LD or the ECL) was split into two paths using a 3-dB fiber optic coupler. One path passed through a Mach-Zehnder modulator (MZM) driven by a 2.5 GHz RF signal, shifting the detection frequency away from 0 Hz in the RF spectrum analyzer for improved accuracy. The other path traversed a 5-km SMF-28 fiber delay line with a polarization controller (PC), ensuring uncorrelated laser light after the long delay. The resulting beat note, centered at 2.5 GHz, was recorded using an avalanche photodiode (APD) connected to an RF spectrum analyzer. The interference between the two optical paths results in the APD photocurrent comprising direct intensity detection and heterodyne frequency mixing components. Consequently, the laser spectrum auto-correlates with its delayed version, exhibiting a 3dB linewidth twice that of the original laser in the frequency domain autocorrelation function. The measured

linewidths using the delayed self-heterodyne method are shown in Figure 5(d), where both the ECL and injection-locked FP-LD demonstrate linewidths below 50 kHz, ensuring low phase noise performance in coherent systems. This validates the low-cost FP-LD's ability to inherit the narrow spectral linewidth characteristic from the OIL parent laser through injection locking.

2.2. Cost-Effective TFDM Coherent PON Enabled by Optical Injection Locking

Utilizing OIL in a coherent PON can result in significant cost savings for optical hardware such as light sources. However, in a conventional TDM coherent PON with a single feeder fiber configuration, an optical master tone for OIL can overlap with downstream coherent signals, leading to transmission errors. A two-fiber optical distribution network (ODN) adds substantial deployment costs and is often avoided. The TFDM coherent PON approach described earlier in this paper enables coupling the optical master tone between two adjacent subcarriers, facilitating low-cost optical network unit (ONU) devices through OIL in a single fiber configuration.

Figure 6 illustrates the overall structure of the TFDM PON. In this example, in the DS direction two subcarriers each running at 50 Gb/s (12.5 GBd dual polarization (DP)-quadrature phase shift keying (QPSK) signal) for an aggregated data rate of 100 Gb/s are generated over a single wavelength at the optical line terminal (OLT) and broadcasted continuously. The DS TFDM subcarriers are coupled with two optical tones whose center frequencies are at f_1 and f_2, respectively. The frequency spacing between the optical tones f_1 and f_2 is 100 GHz, to align with the ITU DWDM frequency grid. The first optical tone at f_1, which shares the same frequency as the optical carrier of the DS TFDM signals, is used as the master light source for OIL to generate LO and detect the DS signals at the ONU. In the US direction, four TFDM subcarriers are used for signal transmission in TDM burst mode (details in coherent burst reception will be discussed in Section 3), each running at 25 Gb/s capacity (6.25 GBd DP-QPSK signal) for an aggregated data rate of 100 Gb/s. The second optical tone at f_2 is used as the master light source for OIL to produce an optical carrier at the ONU for US signal transmission. It is important to mention that the OIL process amplifies the optical power of both tones; as a result, extra optical amplifiers are not required. Leveraging both time and frequency domain processing in the US direction, data can be multiplexed in two-dimensional bandwidth resource blocks, providing great architectural flexibility. For instance, in certain applications when services with minimal latency and disruption are required, consecutive short bursts from different ONUs can be configured dynamically in one of the TFDM subcarriers to minimize transmission latency.

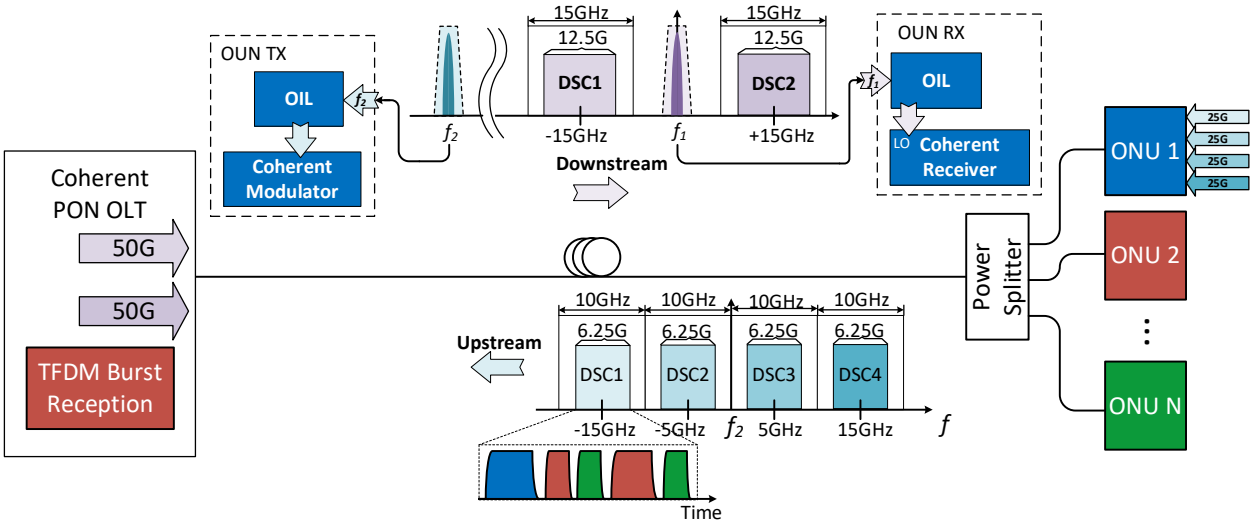

Figure 6 – Coherent TFDM PON architecture featuring remote optical tone delivery and upstream burst

Experimental configuration of the TFDM coherent PON is displayed in Figure 7(a). At the OLT side, two ECLs are used as light sources, one (191.7 THz) to generate DS TFDM signals that consist of two subcarriers through a coherent driver modulator (CDM), while the other (191.6 THz) provides the OLT receiver's local oscillator (LO) for US signal detection. The output of the two ECLs is also coupled with the TFDM signals and transmitted downstream to provide optical master tones for injection locking at the ONUs. For demonstration purposes, an ODN consisting of a 50 km fiber link and a 1×32 passive optical splitter is used in the experiment. At the ONU end, a multiport tunable optical filter (TOF) separates the DS TFDM signals and the two optical tones. The 191.7 THz optical tone is used to generate an LO through OIL process for a coherent homodyne receiver to detect DS TFDM signals. The other optical tone at 191.6 THz is employed to produce an optical carrier for US TFDM burst signal transmission through another OIL setup that is coupled to a CDM. Both DS and US TFDM signals are processed through offline DSP codes. The optical spectra of the DS and US TFDM signals are depicted in Figure 7(b) and Figure 7(c), respectively. Figure 7(d) and Figure 7(e) illustrate the optical spectra of the FP-LD before and after the injection locking process, respectively. Although off-the-shelf products are used extensively in this experimental demonstration, to achieve low-cost commercial products especially for ONUs, it is feasible to combine these components on advanced photonic integration platforms.

(a)

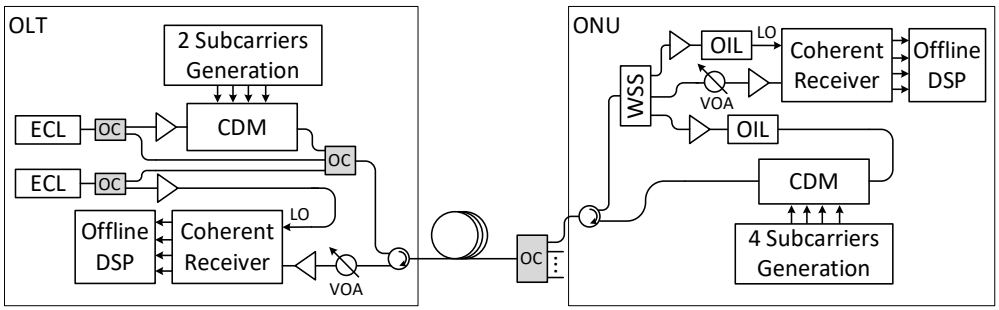

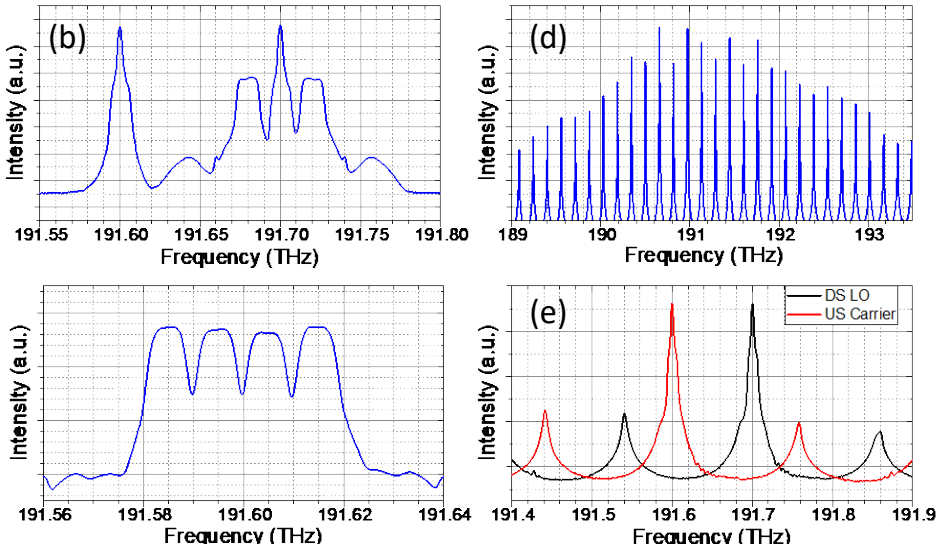

Figure 7 – (a) Experimental setup; (b) spectrum of TFDM DS subcarriers and two optical tones; (c) spectrum of TFDM US burst subcarriers; (d) free-running FP-LD spectrum; (e) injection locked FP-LD spectrums

To demonstrate system functionality and performance of the TFDM coherent PON architecture with remote optical carrier delivery, bi-directional transmission tests have been performed through the 50 km/32 split ODN. Figure 8(a) and Figure 8(b) show the performance of the DS transmission bit-error-rate (BER) versus received optical power (ROP) per channel for each of the two 50 Gb/s TFDM subcarriers, respectively. For DS direction, the TFDM signals are transmitted in continuous mode for broadcasting, with injection locked FP-LD used as LO for ONU receiver. As references, Back-to-back (B2B) BER versus ROP per channel results using the OIL LO are included in each plot, together with fiber transmission and B2B results using regular ECL as ONU receiver LO. Staircase hard-decision (HD) forward error correction (FEC) threshold (BER=4.5E-3) and concatenated soft decision (SD) FEC threshold (BER=1.2E-2) are also added to each chart. Compared to using conventional ECL as receiver LO, the architecture of using remote optical tone delivery and OIL as ONU LO is functionally proven and shows negligible performance penalty.

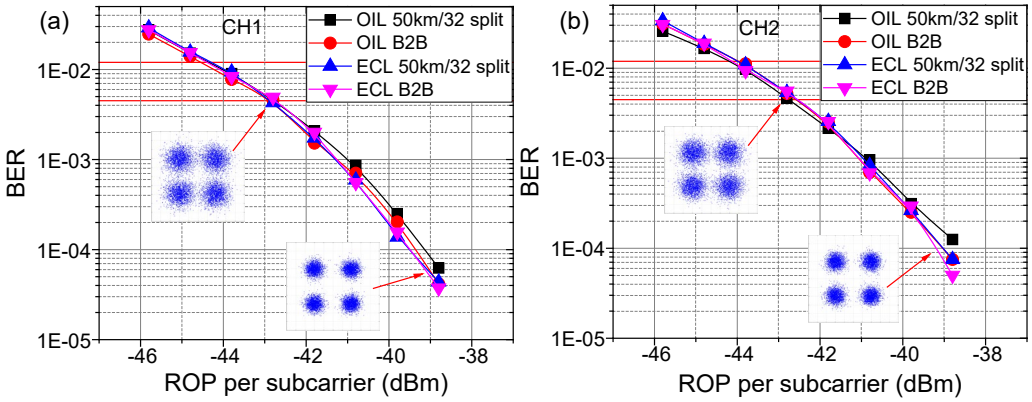

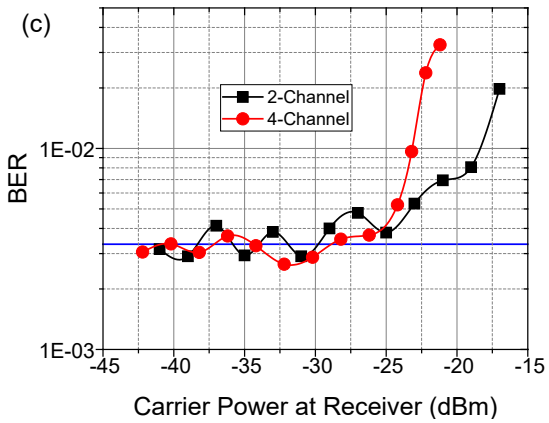

Figure 8 – Experimental results: (a) DS TFDM CH1 (CM); (b) DS TFDM CH2 (CM); (c) optical carrier impact on TFDM signal

Understanding the impact of the optical carrier on the neighboring TFDM subcarrier is crucial. To test the optical tone impact, the optical power of the master tone is gradually increased while the receiver side TFDM subcarrier power is fixed at -40.2 dBm. Figure 8(c) shows the BER performance of a TFDM subcarrier versus the power level of the adjacent optical tone. Two TFDM configurations are tested: the 2-channel and the 4-channel cases as described in Figure 6. A reference of BER = 3.34E-3 when no optical tone is inserted between the TFDM subcarriers is plotted in a red line. From the results, only a negligible performance degradation is observed when the optical tone power is within -25 dBm, and closer-spaced TFDM subcarriers tend to be more sensitive to the increment of the optical tone power. By optimizing the FP-LD for robust injection locking under low injection power (i.e., < -25 dBm), the system can be further simplified by removing the TOF port at the ONU receiver without degrading the DS TFDM signal performance.

Using an OIL-based ONU Tx laser enabled by the remotely delivered optical tone, BER versus ROP per channel results for US burst TFDM signals are shown in Figure 9(a)-(d). The results include both fiber transmission (50 km/32 split) and B2B cases, as well as the BER performance of the four subcarriers using regular ECL as Tx laser in comparison. Similar to the DS broadcasting results, the US burst transmission using the OIL-based transmitter exhibits negligible performance degradation at both the staircase HD FEC threshold (BER=4.5E-3) and concatenated SD FEC threshold (BER=1.2E-2), compared with the traditional ECL-based transmitter.

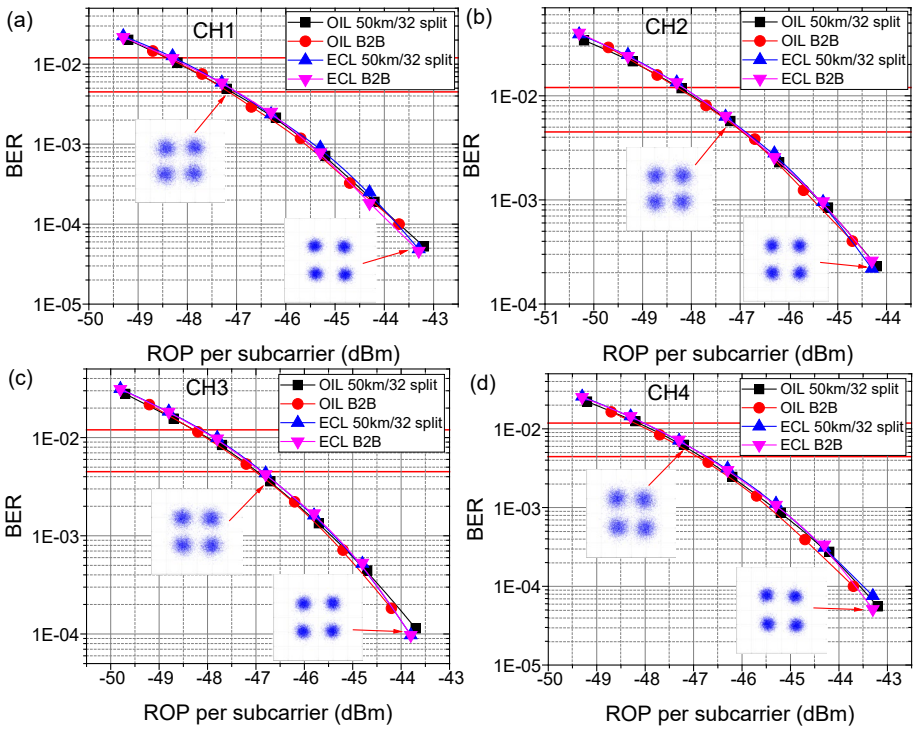

Figure 9 – Experimental results: (a) US TFDM burst CH1; (b) US TFDM burst CH2; (c) US TFDM burst CH3; (d) US TFDM burst CH4

An additional benefit of the OIL-based system is that both ONU Tx and Rx LO are frequency locked to the OLT light sources, which guarantees minimal optical frequency offset between ONU and OLT. Based on experimental results, the regular ECL-based system contains a carrier frequency offset (CFO) on the order of 0.34 GHz, making signal recovery impossible without CFO compensation. In comparison, the OIL-based system only contains a CFO of 0.12 MHz due to a reliable frequency locking between the OLT and ONU lasers. This minimal residual CFO in the architecture allows for simplification of the Rx coherent DSP by removing the CFO compensation process without significant performance degradation. Compared to a traditional ECL-based system that includes CFO compensation, the TFDM coherent PON leveraging OIL offers almost identical performance while significantly simplifying the Rx DSP complexity in addition to ONU hardware cost savings.

3. Coherent Upstream Burst Transmission and Detection in PON

As discussed previously, when designing next-generation optical access networks that require 100 Gb/s and higher capacities, single-wavelength Time Division Multiplexing (TDM) coherent PON is a promising solution. However, realizing efficient upstream burst-mode coherent detection remains a key challenge, as conventional continuous-mode techniques used in point-to-point links are inadequate due to the long acquisition time required for signal recovery. In this section, we demonstrate a robust, high-efficiency preamble design and burst-mode DSP approach for 100 Gb/s/λ TDM coherent PON upstream detection. By sharing the preamble unit across multiple DSP functions such as frame synchronization, state-of-polarization (SOP) estimation, and frequency offset estimation (FOE), the burst preamble length is only 71.68 ns. Robust performance under large frequency offsets, residual fiber dispersion, and long-term operation is confirmed. Using this short preamble, 100 Gb/s DP-QPSK upstream burst detection is achieved with 36 dB power budget over 50 km fiber and 40 dB dynamic range. This approach offers reliable burst-mode detection while reducing complexity and costs compared to prior semi-coherent efforts that compromise sensitivity or require non-standard transceivers [21, 22].

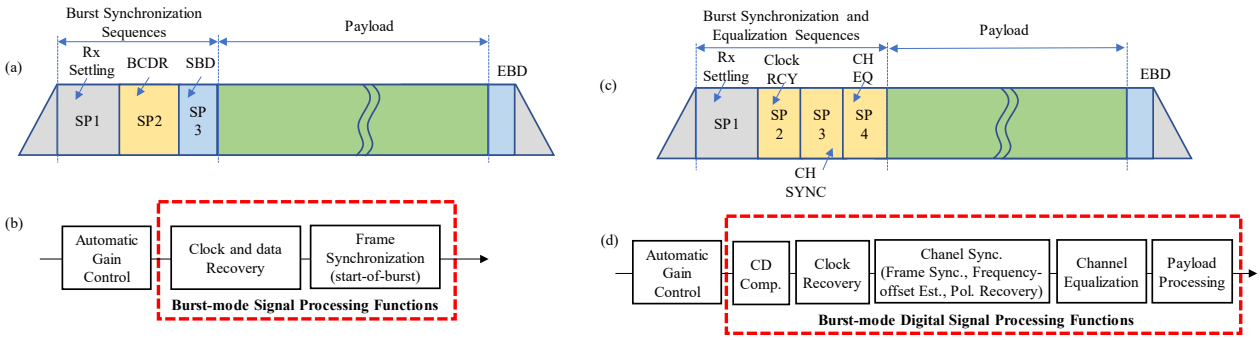

Figure 10 – The schematic principles: (a) and (b) are the burst frame structures and upstream burst-mode signal recovery functions for traditional IM-DD PON; (c) and (d) are the burst frame structures and upstream burst-mode signal recovery functions for CPON

The burst-mode detection in coherent TDM-PONs presents significant challenges compared to traditional direct-detection PONs. As illustrated in Figure 10 (a) and (b), while intensity-modulation direct-detection (IM-DD) PONs require burst synchronization patterns (SPs) for functions like automatic gain control, burst clock and data recovery, and frame synchronization, coherent PONs necessitate additional operations to handle the complexities of phase, polarization, and amplitude modulation. Coherent upstream burst detection demands processing of signals with different clocks, carrier frequency offsets, carrier phases, SOPs, and channel responses from various ONUs. The preamble design shown in Figure 10 (c) and (d) incorporates four SPs: SP1 for receiver settling and automatic gain control; SP2 for digital clock recovery; SP3 for channel synchronization encompassing frame synchronization, frequency offset estimation, and SOP estimation for polarization separation; and SP4 for channel adaptive equalization. The corresponding burst-mode DSP functions, implemented after analog-to-digital conversion, include digital clock recovery, channel synchronization, and channel response estimation for adaptive equalizations. The order and combination of these functions can vary based on the employed algorithms, with frame synchronization often preceding channel synchronization due to the requirement for accurate starting positions in training sequence-based algorithms. This robust and efficient preamble design, combined with data-assisted burst-mode DSPs, addresses the challenges of coherent upstream burst-mode detection in high-capacity TDM-PONs.

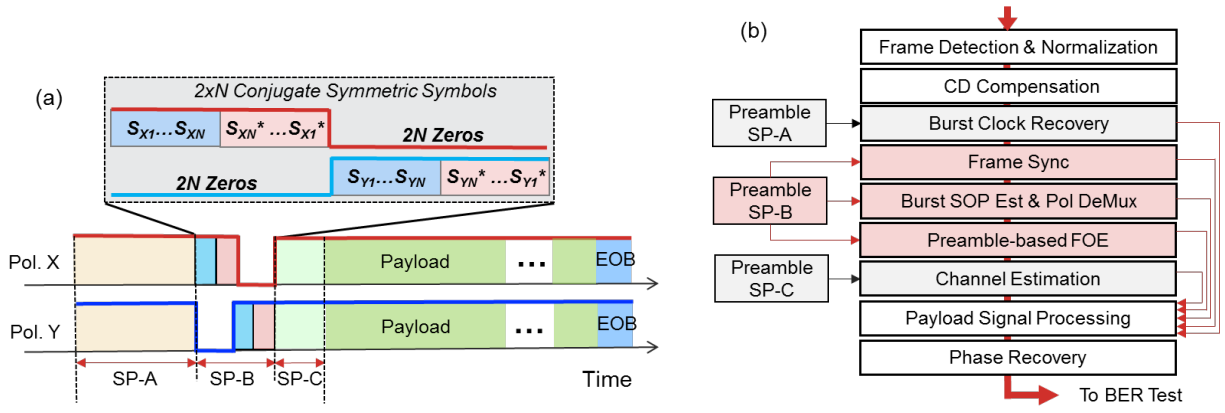

Figure 11 (a) the high-efficient preamble design and (b) the corresponding data-aided burst-mode DSP for 100G CPON

Figure 11(a) depicts our upstream frame structure with a preamble designed for burst transmission, while Figure 11(b) illustrates the corresponding burst-mode DSP flow after receiver settling. Focusing on the burst-mode DSP part based on the designed preamble units, the overall flow is structured in a feed-

forward manner to reduce processing latency and shorten the preamble length. Following normalization and non-data-aided chromatic dispersion compensation (CDC), five essential data-aided DSP functions are performed, as shown in Figure 11(b), based on three synchronization patterns: SP-A, SP-B, and SP-C.

SP-A is employed for burst clock recovery utilizing DC-balanced, state-near-equally distributed QPSK symbols, with the fast square-timing-recovery algorithm [14] applied based on the received symbols within the SP-A section. Notably, the pattern used in SP-A can also be leveraged for burst-mode automatic gain control with an extended overall length. Since the square-timing-recovery algorithm is not training-based, accurate frame synchronization is unnecessary.

The most notable unit is SP-B, specially designed to perform three key data-aided DSP functions: frame synchronization, SOP estimation, and FOE. By sharing the same preamble unit, the overall preamble length is reduced. Frame synchronization is implemented first, as other functions rely on the training sequence and require precise frame synchronization. The frame synchronization algorithm must be tolerant of carrier frequency offsets. SP-B comprises 4N symbols, including 2N conjugate symmetric symbols and 2N zeros on each polarization, as shown in Figure 11(a). The pattern [SX, 0; 0, SY] is transmitted, where SX = [sx1, ..., sxN, sxN*, ..., sx1*] and SY = [sy1, ..., syN, syN*, ..., sy1*]. Essentially, the 4N symbols in preamble SP-B are staggered and transmitted with 2N symbols in each polarization. Without inter-polarization crosstalk between X and Y polarizations, accurate frame synchronization is realized by a sliding window with normalized auto-correlation process on each polarization:

$$C_{x,y}(m) = abs[\sum_{k=0}^{N-1} r_{x,y}(m+k)\, r_{x,y}(m+2N+k-1)]/P_N, C(m) = W_x C_x + W_y C_y \quad (1)$$

Let $r_{x,y}$ denote the received signals from the X and Y polarizations, respectively. C_x and C_y represent the normalized auto-correlation functions on each polarization, while $C(m)$ is the combined function for peak search. W_x and W_y are defined as the power ratios of each polarization, e.g., $W_x=P_x/(P_x+P_y)$. This approach enables the precise localization of the SP-B symbols from the received signal. Assuming $[r_{x1},r_{x2};r_{y1},r_{y2}]$ are the received SP-B symbols, the SOP can be instantly estimated. Extending the single polarization case in [23], the inverse Jones Matrix can be estimated as:

$$H = [\sqrt{\alpha_2}e^{-j\gamma_2}, \sqrt{(1-\alpha_2)}\,; -\sqrt{(1-\alpha_1)}, \sqrt{\alpha_1}e^{j\gamma_1}] \quad (2)$$

Where $\alpha_1 = |r_{x1}|^2/(|r_{x1}|^2+|r_{y1}|^2)$, $\gamma_1 = arg(r_{x1}/r_{y1})$, and α_2 and γ_2 can be obtained from the second half of the SP-B symbols. After polarization demultiplexing based on the inverse Jones Matrix, FOE is performed utilizing the training symbols in SP-B. To achieve fast and accurate FOE, a modified maximum likelihood (ML) criteria FOE algorithm [24] is employed, taking into account the two polarizations to estimate the CFO.

Subsequently, SP-C is designed with QPSK symbols for channel estimation based on the constant modulus algorithm (CMA) in the DSP [25]. The information obtained from the preamble is then applied to the payload process, significantly simplifying the payload demodulation. Following phase recovery, BER calculation is performed to measure the performance. In the following experiments, SP1, SP2, and SP3 comprise 1024, 512, and 256 symbols, respectively, resulting in a total preamble length of 71.68 ns (1792 symbols) per burst frame. Additionally, each frame includes a 3.072 μs payload, a 30.72 ns end of burst (EOB), and a 102.4 ns guard interval time separating bursts.

To experimentally demonstrate coherent upstream burst detection in 100-Gb/s/λ TDM coherent PON, burst frames of 25-GBaud DP-QPSK with the preamble were generated at the ONU side using 80-GSa/s arbitrary waveform generators (AWGs) and dual-polarization IQ modulators driven by a 1550nm ECL (<100kHz linewidth). Burst signals from two synchronized ONUs were combined using a 3dB coupler, avoiding collisions through staggered bursts. The combined bursts were transmitted over 50km fiber. At

the OLT, a burst-mode EDFA pre-amplified the signal before coherent detection by mixing with a <100kHz ECL LO in an integrated coherent receiver. The received signals were sampled by a free-running 80-GSa/s digital sampling oscilloscope (DSO) and processed offline using the burst-mode DSPs. The received optical power was varied using a variable optical attenuator (VOA) for BER testing.

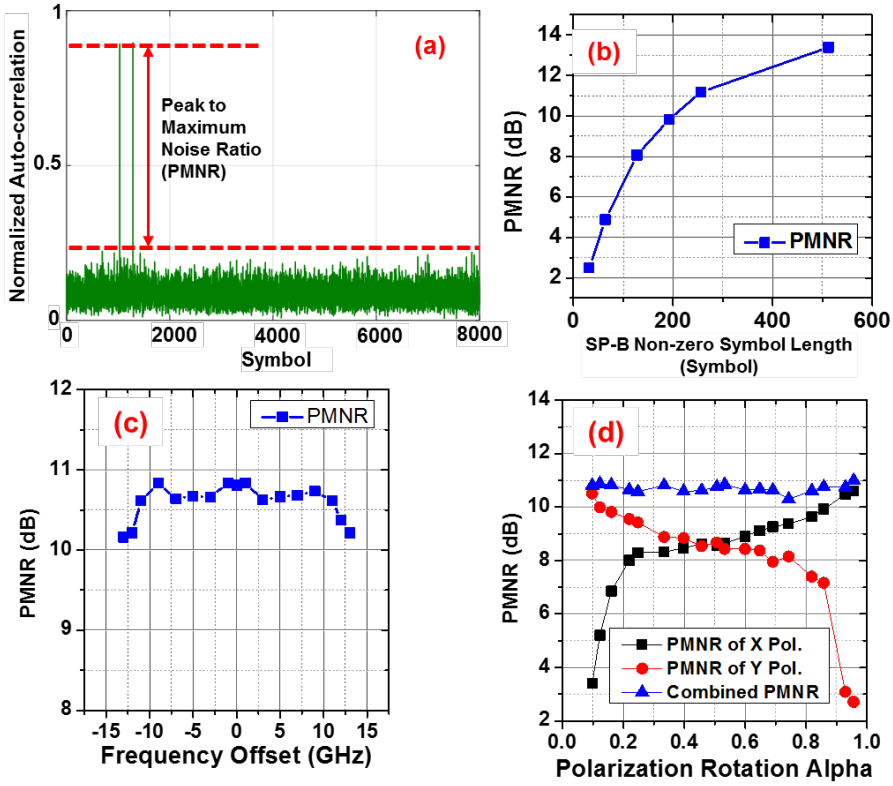

Figure 12 – Experimental results: (a) the normalized auto-correlation output for peak search; (b) the PMNR vs SP-B non-zero symbols length; (c) PMNR vs frequency-offset; (d) PMNR vs different polarization rotations

Since SP-B is the most notable unit in our designed preamble, we initially tested its performance for frame synchronization, SOP estimation, and FOE. Figure 12(a) shows the frame synchronization result based on the combined auto-correlation result of *C(m)*, where the two peaks on the X and Y polarizations sharply indicate the synchronization points. These peak locations represent the start of non-zero SP-B symbols in the received signals. To quantify the frame synchronization performance, we define the peak-to-maximum-noise ratio (PMNR) to evaluate the sync-peak quality compared to noise peaks. Figure 12(b) presents the PMNR results versus the non-zero symbol length, demonstrating that 256 non-zero symbols per polarization in SP-B (512 symbols in total, with 256 zeros) provide over 10-dB PMNR, indicating high-quality peaks. This method for frame synchronization is tolerant of frequency offset errors, verified by the results in Figure 12(c), where over 10-dB PMNR is achieved with a 25 GHz offset range (-12.5 to 12.5 GHz). The performance of frame synchronization under different polarization rotation states is shown in Figure 12(d). While the PMNR from one polarization is polarization-dependent and changes with polarization rotation, the combined PMNR using Eq. (1) is polarization-independent, verifying the tolerance to polarization rotation.

(a) (b)

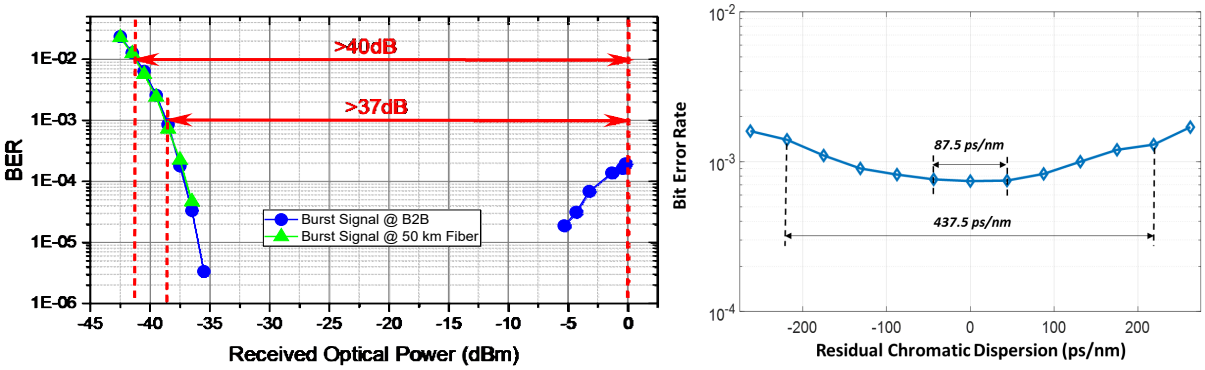

Figure 13 – (a) BER performance versus the received optical power; (b) BER performance as a function of residual chromatic dispersion

The overall signal BER performance versus ROP is presented in Figure 13(a). After 50-km fiber transmission, the required optical power at an average BER of 1×10E-3 is around -38 dBm, and <-41 dBm at BER of 1×10E-2. Leveraging the high receiver sensitivity offered by coherent detection, pre-forward-error-correction (pre-FEC) BER thresholds of 1×10E-3 and 1×10E-2 are used, expecting simpler FEC coding schemes to lower the coding and decoding complexity. The dynamic range of the coherent receiver was also tested. Without changing the receiver setup at the OLT side (same burst-mode EDFA current and integrated coherent receiver setup), >40dB dynamic range of received power was achieved for the 100G coherent PON upstream burst signals at 1×10E-2 FEC threshold, and >37dB at 1×10E-3 FEC threshold. Furthermore, the overall BER performance under different residual chromatic dispersions was evaluated, as shown in Figure 13(b). No obvious BER penalty was observed when the residual dispersion was within ±87.5 ps/nm, while a small BER penalty was observed within ±218.75 ps/nm residual dispersion range. The received optical power was kept at -38.5 dBm during this test.

In conclusion, we have developed and experimentally demonstrated a reliable and efficient preamble design with corresponding burst-mode DSP for coherent upstream burst detection in 100G TDM coherent PONs. The designed preamble's effectiveness and performance under various test conditions was verified. By sharing the preamble unit across multiple DSP functions, the overall length was reduced. Robust performance was confirmed under large frequency offsets and residual chromatic dispersion. Transmission experiment with upstream burst detection indicating that >36dB power budget over 50km fiber was achieved using the 71.68ns preamble and burst-mode DSP.

4. Flexible-Rate Coherent PON up to 300 Gb/s Capacity

Current deployed PONs in access networks operate with a fixed line rate configuration at the physical layer; as a result, the overall peak capacity is constrained by the lowest performing ONU. Typically, existing PONs exhibit limited system flexibility, suboptimal resource utilization, and stringent transceiver design requirements [26]. In our vision, future generation PONs will be capable of offering greater adaptability, enabling adjustable capacity and link budget to more effectively address the varying demands of end-users. Based on the coherent upstream burst preamble and DSP design that was described in the previous section, we introduce a novel flexible-rate coherent PON design that utilizes a low-complexity burst frame detection scheme for modulation format selection. This burst frame detection algorithm and the burst preamble design for various modulation formats are thoroughly analyzed. In laboratory experiments, the method can accommodate a broad spectrum of modulation formats and corresponding link capacities. Leveraging this burst detection scheme, two innovative flexible-rate coherent PON architectures have been experimentally validated. The first architecture employs TDM with three distinct modulation formats for both DS and US transmission. The second architecture integrates an optical frequency comb-based multi-wavelength source for downstream broadcasting and TDM bursts

with three modulation formats for US transmission. Both architectures can achieve a peak data rate of 300 Gb/s transmission through a 50 km / 1×32 split ODN.

4.1. Burst Frame Detection and Modulation Format Identification

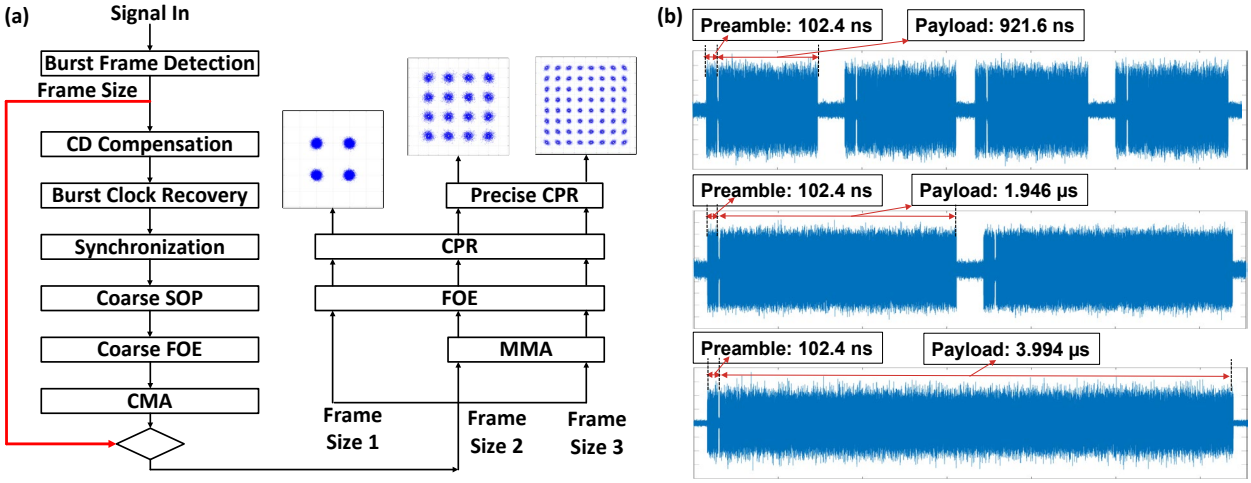

Figure 14 – (a) Coherent DSP with shared processes between different modulation formats and burst frame detection for modulation format identification; (b) burst frame design examples for DP-QPSK, DP-16QAM, and DP-64QAM modulation formats, respectively

Figure 14(a) illustrates the methods for a coherent burst DSP, featuring a burst frame detection algorithm employed at the onset of coherent burst signal reception. This algorithm is utilized to identify the received upstream TDM burst and the corresponding modulation format based on the specific frame size. For demonstration purposes, we employ three modulation formats: dual-polarization quadrature phase shift keying (DP-QPSK), dual-polarization 16 quadrature amplitude modulation (DP-16QAM), and dual-polarization 64 quadrature amplitude modulation (DP-64QAM). Future enhancements could incorporate advanced technologies such as probabilistic constellation shaping (PCS) and adaptive forward error correction (FEC) coding into the scheme, aiming to achieve finer granularity in the net information rate.

The received burst signal is initially stored on a computer hard drive and processed offline using MATLAB. At the start of coherent burst signal reception, a burst frame detection algorithm determines the frame size of the received upstream TDM burst, which is then used to identify the associated modulation format. The burst preamble aids in clock recovery, channel synchronization, and channel equalization, directly passing processed parameters to payload processing without needing full convergence. The preamble is designed to be robust against impairments and efficient in overhead, using a QPSK modulation format as baseline, comprising 2560 symbols at 25 GBaud, which equals 102.4 ns in time. Figure 14(a) outlines the steps: identifying burst frame boundaries using power detection, calculating burst frame size, followed by burst synchronization and equalization sequences incorporating CD compensation, clock recovery, synchronization, SOP estimation, and FOE. Payload signals are processed using traditional coherent DSP, with a shared reception algorithm and first-stage DSP for all three modulation formats until the constant modulus algorithm (CMA) step. For DP-16QAM and DP-64QAM, additional K-means and Gaussian mixture model (GMM) algorithms are included to enhance multi-modulus algorithm (MMA) and carrier phase estimation (CPE) stages. Cascaded CMA and MMA processes handle polarization demultiplexing and channel equalization, followed by CFO compensation and a two-stage Viterbi-Viterbi (VV) algorithm for phase noise reduction. Machine learning based algorithms improve MMA and CPE robustness and accuracy. In the experimental section, MATLAB

code incorporates the described DSP to process received data, with unique burst frame lengths guiding the appropriate DSP steps post-CMA to process different modulation format.

To differentiate the three modulation formats, we created three burst frame design examples, each with a distinct frame size. Figure 14(b) illustrates these designs for DP-QPSK, DP-16QAM, and DP-64QAM modulation formats. The top burst frame design features a 102.4 ns preamble and a 921.6 ns payload section, using DP-QPSK modulation at 25 GBd to achieve a net data rate of 100 Gb/s. The middle design consists of a 102.4 ns preamble and a 1.946 µs payload section, employing DP-16QAM modulation at 25 GBd in the payload section for a 200 Gb/s data rate. The bottom design includes a 102.4 ns preamble and a 3.994 µs payload section, utilizing DP-64QAM modulation in the payload section at 25 GBd to reach a net data rate of 300 Gb/s. For reliable burst signal detection, all designs share the same preamble length and DP-QPSK modulation, with the payload section lengths varied to distinguish between modulation formats and data rates. Post-burst frame identification and length determination guide the necessary DSP steps after the CMA, as shown in Figure 14(a). While Figure 14(b) provides examples for experimental verification, in real applications, each modulation format should not be restricted to a specific frame size. This mechanism can flexibly assign signals with various modulation formats to different burst frames, ensuring distinguishable frame sizes for each modulation format.

4.2. Flexible-rate Coherent PON with TDM Burst DS and US

In this study, we validate the two flexible rate coherent PON architectures that were introduced at the beginning of Section 4. The first architecture, illustrated in Figure 15(a), utilizes coherent burst signals for both DS and US transmission. The transmitters and receivers are identical in both directions, incorporating burst signal transmitting and receiving functions. The Tx setup includes an ECL, a CDM, and a semiconductor optical amplifier (SOA), while the Rx consists of a coherent receiver and offline DSP. This design supports flexible modulation formats for both DS and US without the need for multi-wavelength sources, allowing the use of the same wavelength for both directions. This method, though requiring additional fiber, can be applied in fiber-abundant scenarios to reduce the optical hardware demands, especially in the ONUs, as a single laser (1553.3 nm in this experiment) can handle both DS detection and US signal generation. Signals are generated by an AWG modulating the ECL output through the CDM using 25-GBd DP-QPSK, DP-16QAM, and DP-64QAM modulation formats. These signals are transmitted in TDM bursts, each assigned a specific frame length to support multiple data rates simultaneously: 25600 symbols for DP-QPSK, 51210 symbols for DP-16QAM, and 102410 symbols for DP-64QAM. A coherent homodyne receiver captures the transmitted data, processed offline using MATLAB. The coherent receiver is integrated into an optical modulation analyzer (OMA) with 40 GHz bandwidth, 80-GSa/s ADC sampling rate, and up to 2 Gs/channel memory. A EDFA pre-amplifier amplifies the received signal to around -3 dBm for optimal receiver performance, with a VOA placed before the pre-amplifier for transmission experiments. The ODN includes two 50 km feeder fiber links and a 1x32 passive optical splitter. A two-fiber design in the feeder section, combined with an optical circulator, routes the DS and US signals to mitigate reflection penalties caused by Rayleigh backscattering and lumped reflection in the feeder fiber link [27, 28].

(a)

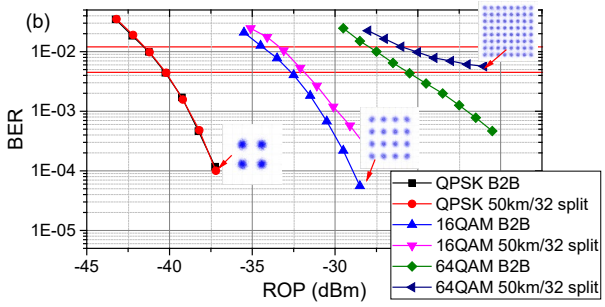

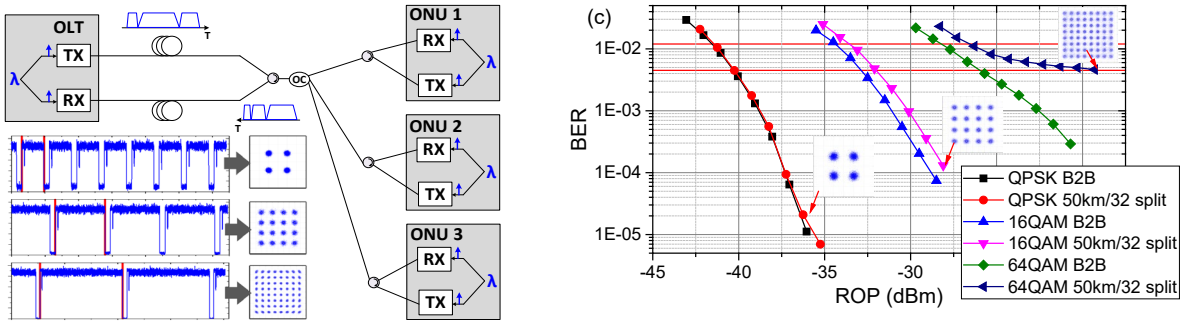

Figure 15 – (a) Flexible rate coherent PON setup with TDM burst DS and US; (b) BER versus ROP in DS; (c) BER versus ROP in US

Figure 15 (b) and (c) illustrate the BER performance relative to ROP for both DS and US transmission using the three modulation formats in this first coherent PON architecture design. The ROP is measured prior to the EDFA pre-amplifier. For reference, the graphs also show B2B BER vs. ROP results, the staircase HD FEC threshold at BER=4.5E-3 [29], and the concatenated SD FEC threshold at BER=1.2E-2 [30]. The functionality of the architecture has been validated through bidirectional transmission utilizing the TDM scheme in this experimental demonstration. Thanks to the two-fiber link, no significant performance degradation from reflections was observed at various data rates. This architecture offers a cost-effective ONU solution, supporting flexible data rates while effectively mitigating reflection penalties in single-wavelength bidirectional transmission for coherent PON.

4.3. Flexible-rate TWDM Coherent PON

The second architecture integrates time and wavelength division multiplexing (TWDM) over a single fiber link, as depicted in Figure 16(a). This setup supports DS signals at 100 Gb/s, 200 Gb/s, and 300 Gb/s in continuous mode, while the US signal is transmitted in TDM bursts. On the OLT side, an optical frequency comb is generated using an ECL with a linewidth of less than 50 KHz and an output power of 15 dBm at 1563.46 nm. The ECL connects to a phase modulator (PM) and a Mach-Zehnder modulator (MZM), both driven by a 25 GHz RF signal, producing an optical frequency comb with 25 GHz spacing between tones [28]. Amplified to approximately +5 dBm by a single-channel EDFA, four comb tones are selected with 50 GHz spacing (λ1: 1563.46 nm, λ2: 1563.86 nm, λ3: 1564.26 nm, λ4: 1564.66 nm) using a wavelength-selective switch (WSS), each with -8 dBm power at the WSS output. Each of the first three tones (λ1-λ3) is sent to an OIL setup that includes a PC, an optical circulator, and a FP-LD. In this setup, comb tones serve as the parent source. Custom FP-LDs from our vendor, housed in 7-pin butterfly packages with 350 µm cavity length and +13 dBm output power, are used. These FP-LDs feature enhanced direct modulation bandwidth up to 10 GHz and include thermoelectric coolers (TEC) for precise temperature control. Through OIL, when the parent tone's wavelength is within ±10 GHz, the child FP-LD locks to the parent tone, achieving frequency and phase synchronization. The injection-locked FP-LDs, with spectral linewidth similar to the ECL, serve as coherent light sources for signal generation and detection. The OIL output (+13 dBm) feeds into a coherent transmitter with a CDM and SOA to generate DS signals using 25-GBd DP-QPSK, DP-16QAM, and DP-64QAM modulation formats. The SOA adjusts the transmitter output power to around +5 dBm. The fourth tone (λ4) is used as an LO for US signal detection. The optical frequency comb source used here is for demonstration; commercial applications would favor lower-cost solutions like integrated quantum dot coherent comb lasers [31]. The ODN comprises a 50 km fiber link and a 1x32 optical splitter. ONUs can choose desired DS data rate by adjusting their LO wavelength, while US transmission uses specific TDM frame lengths for each modulation format. This system operates as a flexible-rate coherent PON, efficiently utilizing fiber resources for both DS and US transmission. A VOA is placed before the optical pre-amplifier and the

OMA for transmission experiments. The ONU Tx includes an ECL, CDM, and SOA, while the Rx includes a coherent receiver and offline DSP.

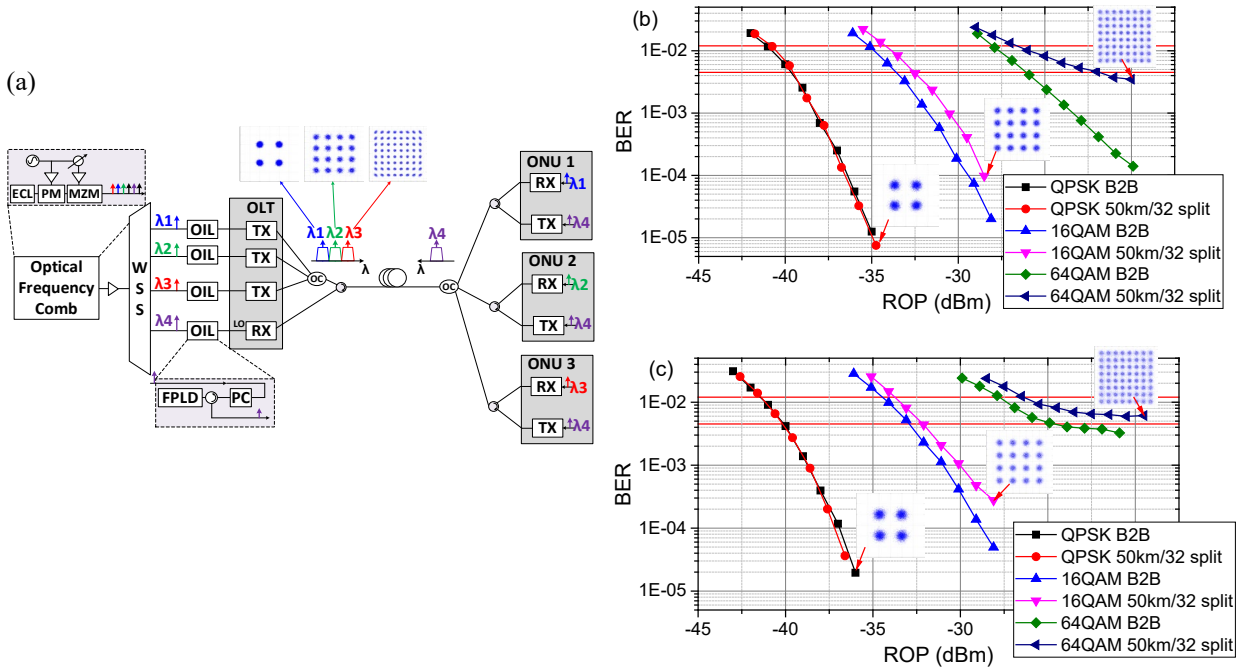

Figure 16 – (a) Flexible rate TWDM coherent PON setup with broadcast DS transmission and TDM burst US transmission; (b) BER vs. ROP in DS; (c) BER vs. ROP in US

Figure 16(b) depicts the BER performance relative to the ROP for DS transmission using wavelengths λ1, λ2, and λ3 from the optical frequency comb source carrying 25-GBd DP-QPSK, 25-GBd DP-16QAM, and 25-GBd DP-64QAM signals, respectively. OIL lasers are used in the OLT transmitters, while LO wavelengths in the ONUs are adjusted to receive the desired DS signals. Similarly, Figure 16(c) shows the BER performance versus ROP for TDM US transmission, using an OIL laser as the LO in the OLT receiver. For comparison, the graphs include B2B BER vs. ROP results, as well as the staircase HD FEC [29] and concatenated SD FEC threshold [30]. The flexible-rate coherent PON architecture's system performance has been validated, with the single fiber design efficiently utilizing fiber resources. Compared to the first architecture (Figure 15(a)), which used conventional ECLs for DS transmitters and US LOs, the current architecture utilizes OIL light sources for DS transmitters and US LOs. Both architectures exhibit similar Rx sensitivity at the concatenated SD FEC threshold of 1.2E-2. For DP-QPSK, the Rx sensitivity at the SD FEC threshold is approximately -41.5 dBm, with minimal impact from fiber transmission effects. Similarly, for DP-16QAM, both architectures show comparable Rx sensitivity at approximately -34 dBm for a 50 km fiber transmission, incurring a 0.8-1 dB fiber transmission penalty compared to B2B conditions. Under DP-64QAM, both architectures exhibit an Rx sensitivity at the SD FEC threshold of approximately -26.5 dBm for a 50 km fiber transmission, with a 1.4-1.6 dB fiber transmission penalty relative to B2B results. A notable difference between the architectures is observed in US transmission with DP-64QAM modulation. The second architecture, utilizing OIL as the LO, shows an error floor, mainly due to the limited output power of the OIL light source (approximately +13 dBm), contrasting with the higher output power of a standard ECL (exceeding +15 dBm). While OIL light sources in the DS direction do not significantly impact Rx sensitivity, their relatively lower output power slightly reduces the link budget.

5. Coherent PON Mutual Protection Enabled by Optical Frequency Comb and Injection Locking

As PON data rates evolve towards 100 Gb/s and higher per wavelength, protecting key network components to avoid service interruptions is increasingly critical due to the surge in traffic and bandwidth demands. Emerging applications such as remote health monitoring, telerobotic surgery, autonomous vehicles, and home security require uninterrupted access services [27, 28]. In the industry, availability, defined as the fraction of time a system operates as intended, is often the key metric for reliability. For a given system, availability can be expressed as:

$$A = 1 - \sum_i^N MTTR_i/(MTBF_i + MTTR_i) \qquad (3)$$

Availability of a PON depends on mean time between failures (MTBF) and mean time to restore or repair (MTTR). The failure in time (FIT), inversely proportional to MTBF, is calculated as FIT = 10^9 / MTBF. The industry goal is to achieve 99.999% availability, meaning less than 5 minutes and 15 seconds of downtime annually. However, current PON protection schemes often involve complex optical switches, control units, or redundant devices like OLTs and backup fiber links, leading to increased deployment costs. Consequently, optical access networks are often poorly protected or unprotected.

To address this for the next generation coherent PON, we demonstrate a cost-effective, mutually protected coherent PON architecture leveraging optical frequency combs, OIL, and remote optical carrier delivery technologies. This approach ensures the protection of critical components, such as OLTs and feeder fibers, in adjacent coherent PON networks by interconnecting passive nodes without complex switching devices or redundant OLTs. The adoption of optical frequency combs and OIL reduces the number of high-cost lasers required, while remote optical carrier delivery ensures fast service restoration without wavelength switching for all ONUs. This system's performance and protection mechanism have been validated in the lab through bi-directional transmission of 100 Gb/s coherent signals over a 50 km fiber link and cascaded passive splitters, demonstrating robust operation in both normal and protection modes.

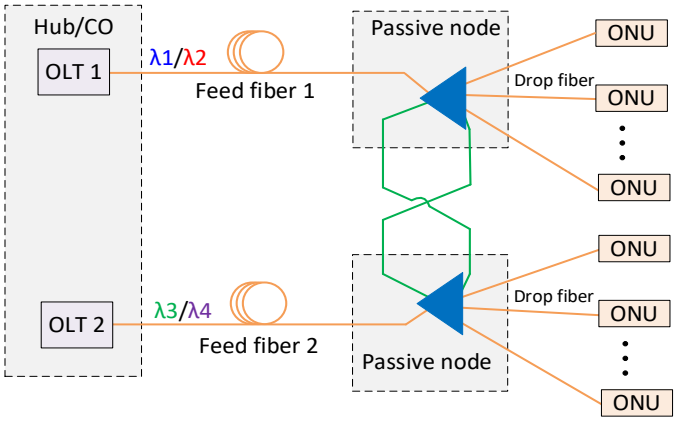

Figure 17 – CPON protection design schematic

Figure 17 illustrates the high-level architecture of the mutually protected coherent PON with OLT and feeder fiber protection. Leveraging the high power budget and wavelength tunability of coherent optics, adjacent coherent PONs can protect each other by connecting the passive nodes. Under normal operation, the two networks operate at different wavelengths (λ1/λ2 for one and λ3/λ4 for the other) to prevent interference. Normal feeder and drop fiber links are shown in orange, while protection fiber links are in green. If a feeder fiber or OLT device fails (e.g., OLT1/fiber link 1 is down), protection activation signals prompt all ONUs in the affected network to switch to the wavelengths of the neighboring network

(λ3/λ4). Consequently, OLT2 will handle DS and US signals for all ONUs. This architecture, scalable to multiple networks, uses 2×(N+1) optical splitters, where N is the number of ONUs per link, and allows flexible protection with asymmetric splitting ratios. Coherent transceivers enable wavelength adjustments for transmitters and LOs, ensuring fast and efficient network recovery.

Table 1- Failure rates and repair time for PON components

	FIT	MTTR
OLT	2500	4 hrs.
ONU	256	24 hrs.
Feeder Fiber	50km x 200/km	24 hrs.
Drop Fiber	2km x 200/km	24 hrs.
Splitter	100	8 hrs.

Table 1 shows statistical failure rates and mean repair times for PON components, indicating that an unprotected PON with a 50 km fiber link can only achieve 99.959% availability. However, with the protection scheme shown in Figure 17, MTTR for the feeder fiber and OLT can be reduced from hours to minutes or seconds, enabling the system to meet the 99.999% availability goal.

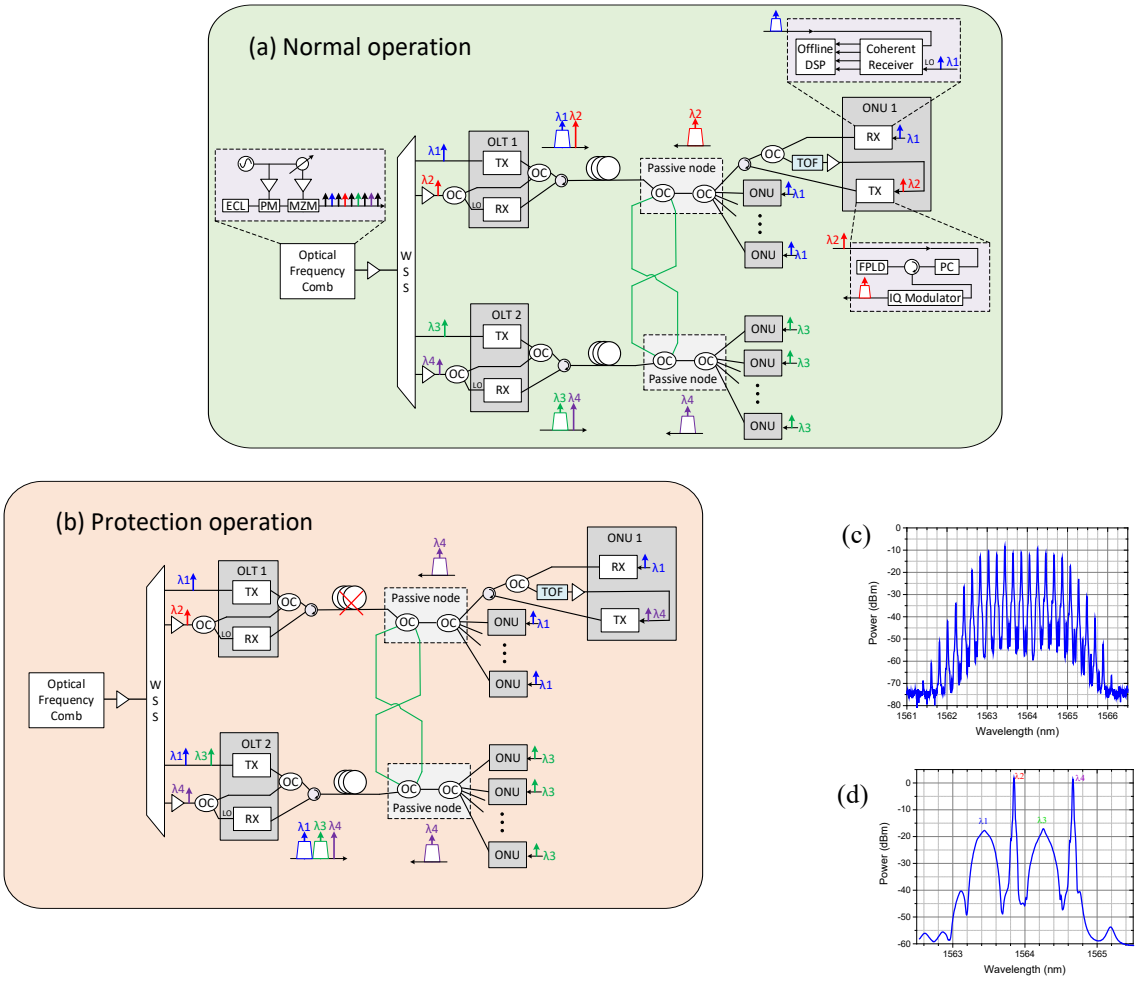

Figure 18 – Experimental setup of mutual protected P2MP networks: (a) normal operation; (b) protection operation; (c) optical spectrum of frequency comb; (d) optical spectrum of coherent signals and remotely delivered carriers

The mutual protection scheme leveraging existing coherent optics faces challenges due to commercial products not being optimized for fast wavelength switching, making it difficult to change US and DS operating wavelengths for all ONUs under protection mode. To achieve fast service restoration and reduce hardware costs, this coherent PON protection scheme utilizes an optical frequency comb source to replace costly ECLs and features remote optical carrier delivery via OIL. In this scheme, the frequency comb and two OLTs are co-located in the same hub or central office (CO), as shown in Figure 18(a). In case of OLT or feeder fiber failure, the two coherent PONs provide mutual protection by tuning an optical filter or wavelength selective switch (WSS), without requiring all ONUs to switch wavelengths. Figure 18(b) illustrates experimentation with a commercially available WSS and a tunable optical filter (TOF) in network protection operation, with further improvements possible using ultrafast tuning integrated WSS. With an estimated 50 ms MTTR for OLT and feeder fiber, this scheme achieves 99.9988% availability, and with ONU/drop fiber redundancy can exceed the 99.999% target if needed. In this architecture, an optical frequency comb is generated by modulating an ECL with a phase modulator and MZM, producing four comb tones (λ1: 1563.46 nm, λ2: 1563.86 nm, λ3: 1564.26 nm, λ4: 1564.66 nm) with 50 GHz spacing. In normal operation (Figure 18(a)), OLT1 uses λ1 for DS and λ2 for US, while OLT2 uses λ3 for DS and λ4 for US. Upon failure of OLT1 or its feeder fiber (Figure 18(b)), OLT2 takes over, providing protection through fast WSS switching without ONU wavelength changes. The optical spectra of the frequency comb, and coherent signals and remotely delivered carriers (λ2 and λ4) are depicted in Figure 18 (c) and (d), respectively.

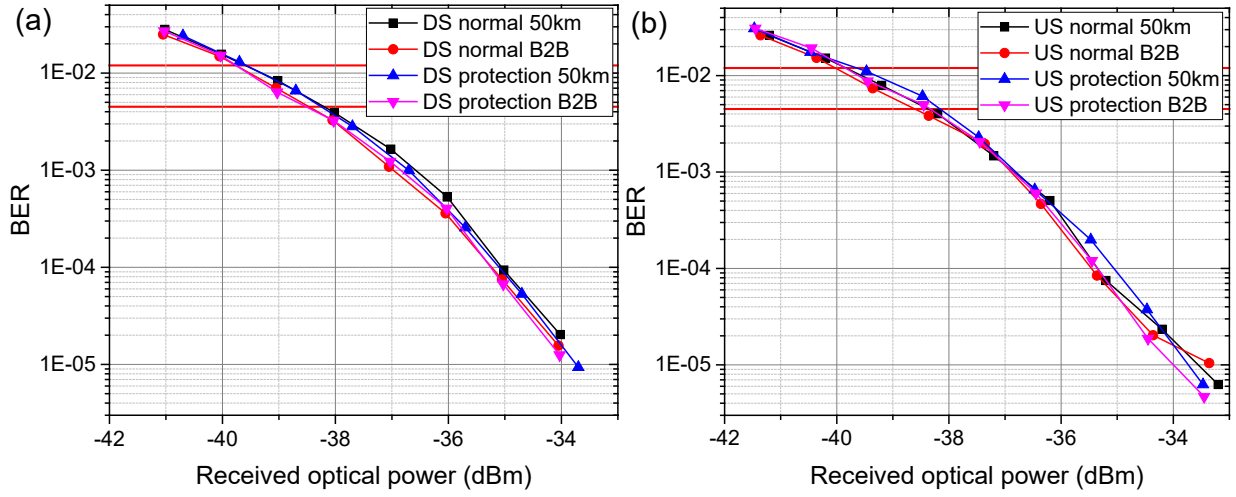

Figure 19 – System performance of the proposed mutual protection scheme: (a) DS BER vs. ROP; (b) US BER vs. ROP

Figure 19 summarizes the experimental results of the network protection design, showing system performance under normal operation and protection mode for both B2B and 50 km fiber link scenarios. Figure 19(a) presents BER versus ROP performance for DS transmission using a 30-GBd DP-QPSK coherent signal. Figure 19(b) shows BER versus ROP performance for US transmission. Tests were conducted using a VOA to adjust the received optical power at the coherent receiver, with HD FEC and SD FEC thresholds plotted in red. Results indicate that system performances under normal operation and protection mode are very similar, with negligible penalty observed.

6. Conclusion

In this article, we provide a comprehensive overview of the cutting-edge advancements in coherent PON, highlighting the significant advantages of coherent optics over legacy IM-DD PONs. Coherent optics offer higher link budgets, increased capacity, and robustness against fiber transmission impairments,

making them superior for next-generation optical access networks. CableLabs initiated the development of coherent PON specifications in 2021, releasing the 100G Coherent PON Architecture Specification in 2023. Current efforts focus on defining the physical (PHY) and upper layer specifications in collaboration with operator and vendor groups. Parallel to specification development, CableLabs continues to innovate in coherent technologies for access network applications, aiming for cost reduction, increased flexibility, and enhanced survivability for higher bandwidth demands.

This article presents CableLabs' latest advancements in coherent PON, including low-cost ONU designs, efficient and robust coherent upstream burst processing, adaptive modulation, flexible data rates, and new protection schemes. It provides an in-depth study of OIL and its applications in coherent PON, demonstrating the ability of using low-cost optical light sources in ONUs while maintaining high system performance. An innovative coherent TFDM PON architecture leveraging OIL is introduced, significantly reducing ONU hardware costs. The article also details the development of a robust coherent upstream burst scheme with advanced preamble design and Tx/Rx DSP, crucial for the success of coherent PON. Experimental demonstrations of two coherent PON architectures with flexible and adaptable data rates, achieving peak data rates up to 300 Gb/s, are highlighted. Additionally, a highly innovative network protection strategy for coherent PON employing a cost-effective mutual protection scheme is presented, enhancing network reliability and resiliency.

In summary, this article showcases the progressive evolution of optical access networks driven by coherent PON technologies. By leveraging innovations such as OIL for cost-effective ONU designs, advanced burst processing for coherent upstream transmission, and flexible data rates, the way is being paved for future advancements in coherent optical access networks. The implementation of a mutual protection scheme further enhances network reliability and resiliency, ensuring high availability and robustness for next-generation optical access networks.

7. Acknowledgements

Special acknowledgments for fruitful discussions and assistance with all aspects of this study: Dr. Curtis Knittle, Chris Stengrim, Matt Schmitt, Karthik Sundaresan, Steve Goeringer, Dr. Jing Wang, Dr. Karthik Choutagunta, as well as the dedicated members of the CPON Working Group (WG) and Operator Advisory Group (OAG).

Abbreviations

ADC	analog-to-digital converter
APD	avalanche photodiode
AWG	arbitrary waveform generator
B2B	back-to-back
BER	bit error rate
CD	chromatic dispersion
CDC	chromatic dispersion compensation
CDM	coherent driver modulator
CFO	carrier frequency offset
CMA	constant modulus algorithm
CMOS	complementary metal–oxide–semiconductor
CO	central office
CPE	carrier phase estimation
CPON	coherent passive optical network
CPR	carrier phase recovery
DAC	digital-to-analog converter
DCI	datacenter interconnect
DS	downstream
DSC	digital subcarrier
DSP	digital signal processing
DWDM	dense wavelength division multiplexing
ECL	external cavity laser
EOB	end of burst
FEC	forward error correction
FIT	failure in time
FOE	frequency-offset estimation
FP-LD	Fabry-Perot laser diode
FTTH	fiber to the home
FTTP	fiber to the premise
Gb/s	gigabits per second
GMM	Gaussian mixture model
HD	hard decision
IM-DD	intensity modulation and direct detection
ITU-T	International Telecommunication Union Telecommunication Standardization Sector
LO	local oscillator
MMA	multi-modulus algorithm
MTBF	mean time between failure
MTTR	mean time to restore
ODN	optical distribution network
OIL	optical injection locking
OLT	optical line terminal
OMA	optical modulation analyzer
ONU	optical network unit
ONT	optical network terminal
P2MP	point-to-multipoint
PC	polarization controller

PCS	probabilistic constellation shaping
PHY	physical
PMD	polarization-mode dispersion
PON	passive optical network
QAM	quadrature amplitude modulation
QPSK	quadrature phase shift keying
ROP	received optical power
Rx	receiver
SD	soft decision
SOP	state of polarization
TDM	time-division multiplexing
TEC	thermoelectric cooler
TFDM	time-and-frequency-division multiplexing
TWDM	time-and-wavelength-division multiplexing
Tx	transmitter
TOF	tunable optical filter
US	upstream
VOA	variable optical attenuator
VV	Viterbi-Viterbi
WDM	wavelength-division multiplexing
WSS	wavelength selective switch

Bibliography and References

[1] Z. Jia and L. A. Campos, “Coherent Optics for Access Networks,” Routledge & CRC Press, Nov. 01, 2019.

[2] J. Wey and J Zhang, "Passive Optical Networks for 5G Transport: Technology and Standards," J. Lightwave Technol. 37, 2830-2837 (2019).

[3] D. van Veen and V. Houtsma, "Strategies for economical next-generation 50G and 100G passive optical networks," J. Opt. Commun. Netw. 12, A95-A103 (2020).

[4] IEEE 802.3ca, Physical Layer Specifications and Management Parameters for 25 Gb/s and 50 Gb/s Passive Optical Networks, 2020.

[5] ITU-T G.9804.1: Higher speed passive optical networks – Requirements: Recommendation G.9804.1, 2019.

[6] ITU-T G.9804.2, Higher Speed Passive Optical Networks: Common Transmission Convergence Layer Specification, Sept. 2021.

[7] N. Suzuki, H. Miura, K. Matsuda, R. Matsumoto, and K. Motoshima, “100 Gb/s to 1 Tb/s Based Coherent Passive Optical Network Technology,” Journal of Lightwave Technology, vol. 36, no. 8, pp. 1485–1491, Apr. 2018.

[8] J. Zhang and Z. Jia, "Coherent Passive Optical Networks for 100G/λ-and-Beyond Fiber Access: Recent Progress and Outlook," IEEE Network, vol. 36, no. 2, pp. 116-123, 2022.

[9] K. Matsuda, R. Matsumoto, and N. Suzuki, “Hardware-Efficient Adaptive Equalization and Carrier Phase Recovery for 100-Gb/s/λ-Based Coherent WDM-PON Systems,” Journal of Lightwave Technology, vol. 36, no. 8, pp. 1492–1497, Apr. 2018.

[10] M. Luo, D. Wu, W. Li, T. Zeng, L. Zhou, L. Meng, Z. He, C. Li, and X. Li, "Demonstration of Bidirectional Real-Time 100 Gb/s (4×25 Gb/s) Coherent UDWDM-PON with Power Budget of 44 dB," Optical Fiber Communication Conference (OFC) 2019, paper Th3F.2.

[11] D. Welch et al., "Point-to-Multipoint Optical Networks Using Coherent Digital Subcarriers," in Journal of Lightwave Technology, vol. 39, no. 16, pp. 5232-5247, 15 Aug.15, 2021.

[12] J. Zhang, Z. Jia, H. Zhang, M. Xu, J. Zhu and L. A. Campos, "Rate-Flexible Single-Wavelength TFDM 100G Coherent PON Based on Digital Subcarrier Multiplexing Technology," 2020 Optical Fiber Communications Conference and Exhibition (OFC), San Diego, CA, USA, 2020, paper W1E.5.

[13] R. Koma, M. Fujiwara, J.-I. Kani, K.-I. Suzuki, and A. Otaka, “Burst-Mode Digital Signal Processing That Pre-Calculates FIR Filter Coefficients for Digital Coherent PON Upstream,” Journal of Optical Communications and Networking, vol. 10, no. 5, pp. 461–470, May 2018.

[14] J. Zhang, Z. Jia, M. Xu, H. Zhang, L. A. Campos, and C. Knittle, “High-Performance Preamble Design and Upstream Burst-Mode Detection in 100-Gb/s/λ TDM Coherent-PON,” Optical Fiber Communication Conference (OFC) 2020, paper W1E.1.

[15] E. K. Lau, H. Sung and M. C. Wu, "Frequency Response Enhancement of Optical Injection-Locked Lasers," IEEE Journal of Quantum Electronics, vol. 44, no. 1, pp. 90-99, Jan. 2008.

[16] E. K. Lau, L. J. Wong and M. C. Wu, "Enhanced Modulation Characteristics of Optical Injection-Locked Lasers: A Tutorial," IEEE Journal of Selected Topics in Quantum Electronics, vol. 15, no. 3, pp. 618-633, May-June 2009.

[17] Z. Liu and R. Slavík, "Optical Injection Locking: From Principle to Applications," in Journal of Lightwave Technology, vol. 38, no. 1, pp. 43-59, 1 Jan.1, 2020.

[18] M. Xu, Z. Jia, H. Zhang, L. A. Campos and C. Knittle, "Intelligent Burst Receiving Control in 100G Coherent PON with 4×25G TFDM Upstream Transmission," 2022 Optical Fiber Communications Conference and Exhibition (OFC), San Diego, CA, USA, 2022, paper Th3E.2.

[19] H. Zhang, Z. Jia, L. A. Campos and C. Knittle, " Low-Cost 100G Coherent PON Enabled by TFDM Digital Subchannels and Optical Injection Locking," 2023 Optical Fiber Communications Conference and Exhibition (OFC), San Diego, CA, USA, 2023, paper W1I.4.

[20] H. Zhang, Z. Jia, L. A. Campos and C. Knittle, "Cost effective 100G coherent PON enabled by remote tone delivery and simplified carrier recovery for burst processing," 49th European Conference on Optical Communications (ECOC), Glasgow, UK, 2023.

[21] J. Zhang, J. S. Wey, J. Shi and J. Yu, "Single-Wavelength 100-Gb/s PAM-4 TDM-PON Achieving Over 32-dB Power Budget Using Simplified and Phase Insensitive Coherent Detection," 2018 European Conference on Optical Communication (ECOC), Rome, 2018, pp. 1-3.

[22] M. S. Erkılınç, D. Lavery, K. Shi, B. C. Thomsen, R. I. Killey, S. J. Savory, and P. Bayvel, "Comparison of Low Complexity Coherent Receivers for UDWDM-PONs (λ -to-the-User)," J. Lightwave Technol. 36, 3453-3464 (2018).

[23] R. Koma, M. Fujiwara, J. I. Kani, K. I. Suzuki, and A. Otaka, "Burst-Mode Digital Signal Processing That Pre-Calculates FIR Filter Coefficients for Digital Coherent PON Upstream," J. Opt. Commun. Netw. 10, 461-470 (2018).

[24] U. Mengali and M. Morelli, "Data-aided frequency estimation for burst digital transmission," in IEEE Transactions on Communications, vol. 45, no. 1, pp. 23-25, Jan. 1997.

[25] S. J. Savory, "Digital filters for coherent optical receivers," Opt. Express 16, 804-817 (2008).

[26] H. Zhang, Z. Jia, L. A. Campos and C. Knittle, "Experimental Demonstration of Rate-Flexible Coherent PON Up to 300 Gb/s," in Journal of Lightwave Technology.

[27] H. Zhang, M. Xu, Z. Jia, and L. A. Campos, "Frequency Comb and Injection Locking Based Mutual Protections in Coherent Optical Access Network," 2022 Optical Fiber Communication Conference (OFC), paper M1I.5.

[28] H. Zhang, M. Xu, Z. Jia and L. A. Campos, "Mutually Protected Coherent P2MP Networks Enabled by Frequency Comb and Injection Locking," IEEE Photonics Technology Letters, vol. 35, no. 1, pp. 27-30, 2023.

[29] International Telecommunication Union (ITU-T) G.709.2 recommendation.

[30] Optical Interworking Forum 400G ZR standard.

[31] H. Zhang et al., "Quantum Dot Coherent Comb Laser Source for Converged Optical-Wireless Access Networks," IEEE Photonics Journal, vol. 13, no. 3, pp. 1-9, June 2021.